



Experimental investigations on heat transfer enhancement for a high aspect ratio rectangular duct roughened by intersecting ribs with inclined ribs

Ali Hussein F. Theeb, Munther Abdullah

Mechanical Engineering Department, University of Baghdad, Iraq.

Received 6 Feb. 2019; Received in revised form 26 Mar. 2019; Accepted 27 Mar. 2019; Available online 31 March 2019

Abstract

In this work, the effect of the intersecting ribs with inclined ribs on the heat transfer performance and friction factor through a rectangular roughened duct have been experimentally investigated. The chosen aspect ratio of the duct (W/H) was 10 and Reynolds number was in the range between 35,700 up to 72,800. The rib-pitch-to-height-ratio (P/e) and Relative roughness height (e/D_h) were 10 and 0.068 respectively. The inclination of the rib with respect to the flow, generates counter-rotating secondary flow along the span that causes span wise variation of heat transfer coefficient. The fluid enters at the leading zone of the rib and travel to the trailing zone, thus raising heat transfer rate at the leading zone while the trailing zone heat transfer is relatively low. To minimize this effect, longitudinal ribs were suggested to use with the inclined ribs in intersection form. A single longitudinal rib was installed at the center of the plate with parallel to flow, this for Model 2, and two longitudinal ribs were used for Model 3. Using the intersecting ribs lead to induced new vortices at every intersection point in addition to the primary vorticities at the leading corner of the inclined rib. So, the heat transfer at the trailing zone will enhance. Therefore, the model 3 provide highest Nusselt number ratio than model 2 are about 13.19 % and 7.03%, respectively, with respect to that of the model 1 (without intersecting ribs), Also, it can be observed that the model 3 with two Intersecting ribs mostly provides higher overall efficiency indices rather than those of the model 2 and 1.

Copyright © 2019 International Energy and Environment Foundation - All rights reserved.

Keywords: Heat transfer; Enhancement; Intersecting-ribs; Secondary flow.

1. Introduction

Many of thermal systems require an enhancement in the heat transfer rates for saving power exhaustion. Different mechanisms for enhancement the thermal performance have been used up to augment the heat transfer. Therefore, the suitable type of heat transfer enhancement technique can be selected according to the required level of augmentation, geometry, pressure drop and the cost.

The artificial surface roughness in form of ribs have been suggested to use. This type may be used in several engineering applications, such as solar air heater and gas turbines. Specially, so, the internal cooling of gas turbines, is the generality technique which used for cooling the hot parts of turbines by employs interior roughened channels for entering the coolant air in order to absorb the heat from hot parts. Ravi et al. [1] studied many different rib geometries, such as V- shaped, W-shaped and M-shaped ribs in a two-pass stationary square channel. They reported the effect of rib shape on the heat transfer and friction

characteristics. A good review [2-5] have been studied the description of secondary flows induced by the inclined ribs caused higher heat transfer coefficients. In addition to that, these secondary flows generated a spanwise variation in the heat transfer coefficient on the ribbed surface. This variation with high levels of the heat transfer coefficient at leading end of the rib while the trailing end heat transfer is relatively low, as depicted in Figure 1. Chung et al. [6] used an intersecting rib at the center with inclined ribs of 60° attack angle, to overcome the span wise variation of heat transfer. They observed an enhancement in locally heat/mass transfer performance, especially for aspect ratio ($W/H = 2.0$) that shows optimum performance. Also, they suggested to use more than an intersecting rib with a high aspect ratio channel. A studying [7-10] investigated the rib pitch to height ratio. It was showed a large effect in the heat transfer and pressure drop characteristics. They approximately found the optimum value of p/e to be 10. This because that the boundary layer was disturbed due to the flow separation and reattachment and thus it augmented the heat transfer. Kim et al. [11] showed that the shape and location of recirculation and reattachment regions were changed due to the different inlet velocity profiles. Also, they conclude that the profile of fully developed flow was showed the best thermal efficiency, that because of induced a little pressure drop. Gao et al. [12] found a periodic similar distribution between the Nusselt number and the wall heat flux. Also, the high aspect ratio led to a good interaction between the main flow fluid and the fluid in near wall region. Lu and Jiang [13] studied the thermal performance of coolant air in a rectangular duct roughened by inclined ribs. The results showed that the average heat transfer coefficients increase with increasing mass flow rates and decreasing the spacing. Ravi and Saini [14] reported that the maximum enhancement of Nusselt number and friction factor were of 4.52 and 3.13 times with respect to smooth double pass duct. Aliaga et al. [15] observed that a separation-reattachment flow phenomenon occurred at $P/e = 12$ and a single vortex flow enclosed between ribs at $p/e = 5$. They discussed the heat transfer distribution, therefore, they found that best heat transfer coefficient on the middle of top surface of the rib occurred at $P/e = 12$ and at the upstream corner. Also, observed decreasing in heat transfer coefficient monotonically downstream for $P/e = 5$. The main objective of the present work is to experimentally investigate the effect of the intersecting ribs on the heat transfer and friction factor characteristics for a roughened rectangular duct with inclined ribs.

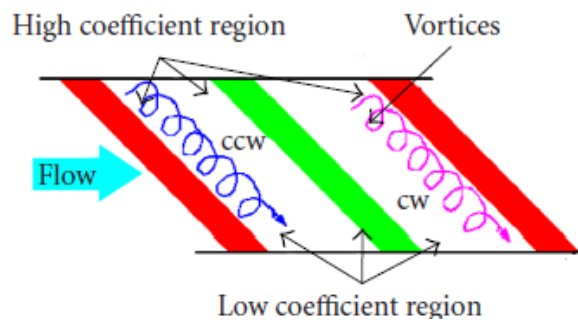


Figure 1. Effect of inclined ribs.

2. Experimental apparatus and procedure

The experiments were carried out in rectangular duct with an open-circuit suction flow. A schematic diagram of the entire experimental set up was presented in Figure 2. The aspect ratio of the duct (W/H) = 10. A bell-mouth is installed at the inlet of the rig supported by a fine-mesh screen inserted to provide a uniform flow with minimum turbulence at the contraction inlet. Air drawn at ambient temperature from the laboratory by a centrifugal blower of 1100W at 2800 rpm located at the downstream end, then enters to the inlet section of the rectangular channel. The channel has a length of 3 m and had been divided into three sections, the first section is (200 cm) long to ensure the flow is fully developed. The test section is (50 cm) long and the exit section is (50 cm) long. The cross section of the channel is 40 cm width by 4 cm. The channel was manufactured using 18 mm thick MDF wood plate. Photographs of the experimental test rig are shown in Figure 3.

A flat plate type heater has been used to provide the bottom surface of test plate with a uniform heat flux. This heater was formed from Mica sheet and electric wire strip with high resistance divided to five pieces. The heater followed by a (50 mm) thickness of fiber insulation layer (Ceramic Fiber Blankets SE / TEK-FIBER). In addition to that covered by (18 mm) wood layer, with apply same insulation procedure for the sides to reduce the thermal losses to ambient.

The test section consisted of polished Aluminum plate of 500 mm length, 400 mm width and 5 mm thick, as shown in Figure 4. The roughness elements (the Aluminum ribs) had been manufactured from the same Aluminum plate that used for the test section. The inclined Ribs had a square cross-section (5 mm × 5 mm). The intersecting rib had the same cross section as the inclined ribs, and it was parallel with the flow direction. These ribs glued manually on the test plate by thermal epoxy only at the ends as a drop to prevent a resistance occurring between the rib and plate.

Pre-calibrated (k-type) thermocouples were used to measure temperatures; sixteen Thermocouples had formed as grid shape for measuring the local temperature of heated top surface. These Thermocouples inserted in holes drilled from the bottom surface of test plate with dimension (1 mm) diameter and (4 mm) depth. Also, three thermocouples had been fixed at the duct walls to measure the duct wall temperature for test section. The temperature of the inlet air was measured by one thermocouple, existed at (5 cm) from the inlet of test section. While, three thermocouples were existed at (5 cm) from the outlet of test section, which used to measure the bulk exit temperature. These thermocouples had been calibrated (The overall accuracy was within ± 0.1 °C) and connected to a digital temperature recorder with a scale division of 0.1 °C. A digital manometer with scale division of 0.001 psi had been used to measure the pressure drop along the test section. The air flow velocity was measured by Hot Wire Anemometer with a scale division of 0.1 m/s and calibrated with Static pitot tube, the maximum error in the flow rate was less than $\pm 4\%$. The heating power to the heater are measured by a digital volt meter with 0.1 V and clamp meter with 0.01 A of division accuracy. Adjust the blower gate to the required air velocity. Switch on the electrical power of the heaters and adjust the power and the test run was allowed, wait for about two hours to reach the steady state condition (stability of the plate surface temperatures), then all measurements are read and record Repeat the above steps for all test models.

3. Roughness geometry and range of parameters

The values of system and operating parameters of this investigation is listed in Table 1. The rib-pitch-to-rib-height ratio (P/e) had been selected as 10, based on the optimum value of this ratio reported by [10]. Similarly, rib height-to-channel hydraulic diameter ratio (e/D_h) is 0.068 [20]. Eight inclined ribs were installed on test surface, with an attack angle of 75° , this for model 1. Then, hybridize the model 1 by an intersecting rib at the center of the plate to form model 2, and model 3 with two intersecting ribs at the sides of the plate, as shown in the Figure 5.

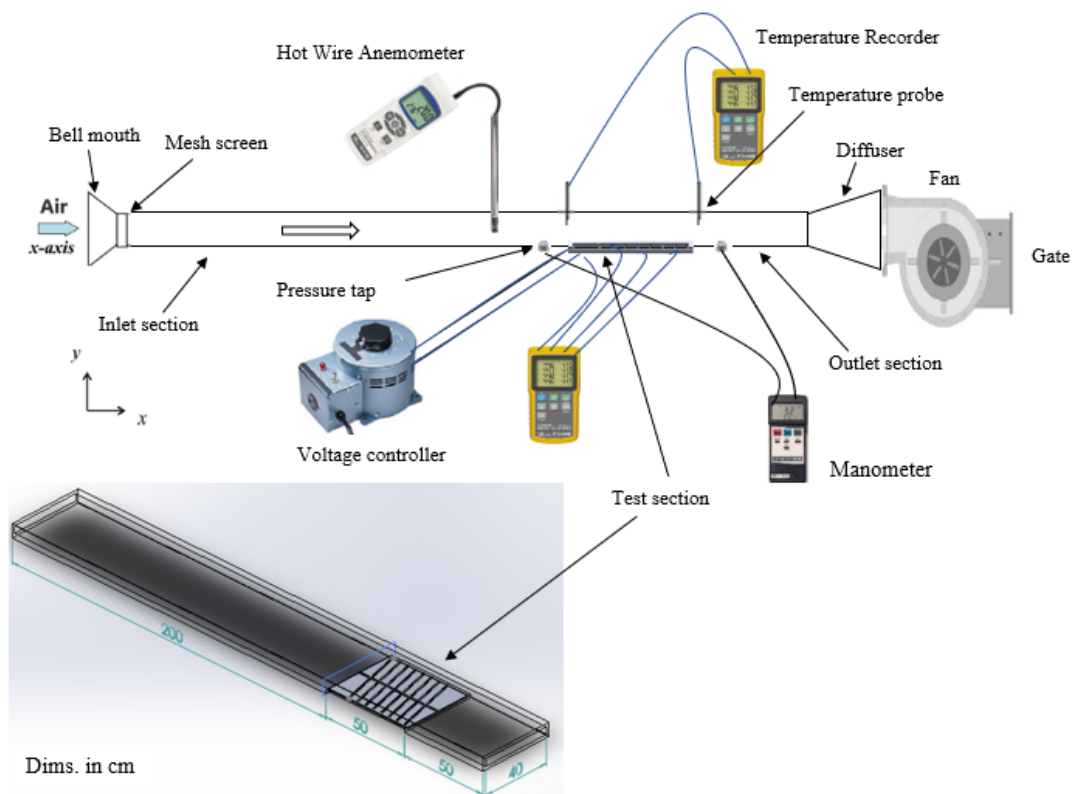


Figure 2. Schematics of experimental setup used in the experiments.

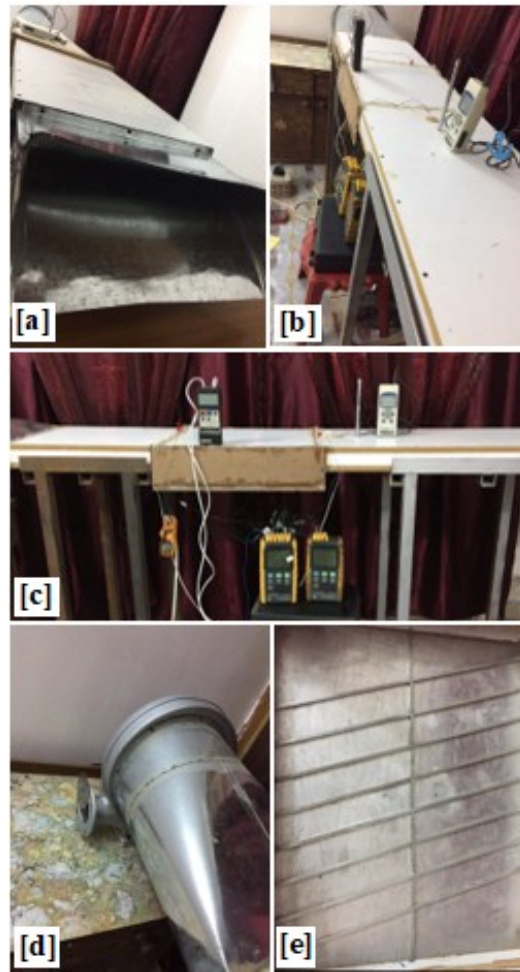


Figure 3. A photograph of the experimental set-up, (a) air intake, (b) inlet section, (c) test section and instrumentations, (d) blower, (e) test plate with attached ribs.

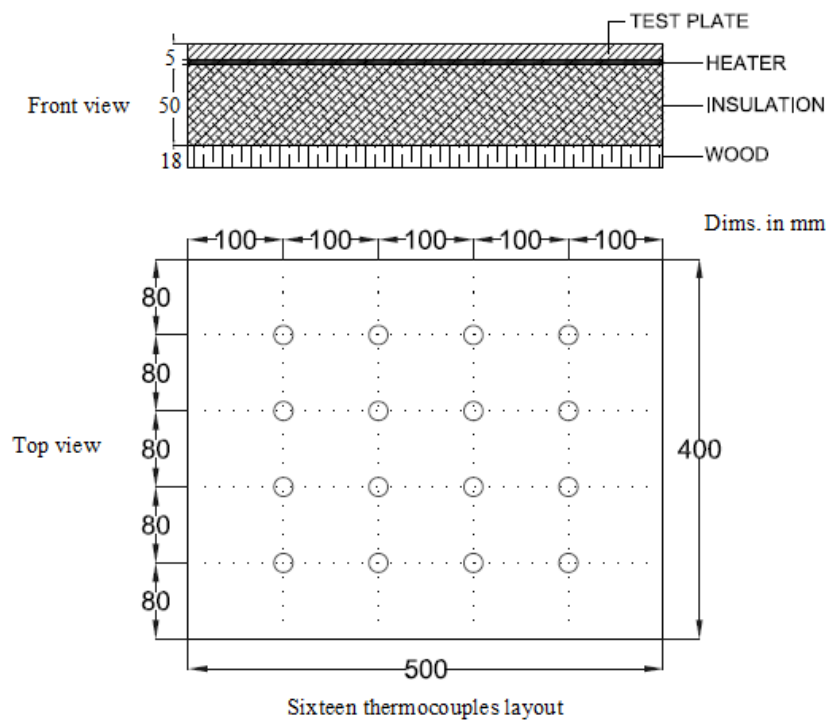


Figure 4. Test section and thermocouples' positions.

Table 1. Values of parameters.

No.	Parameters	Values
1	Relative roughness pitch (P/e)	10
2	Relative roughness height (e/Dh)	0.068
3	Rib height (e) and width (b)	5 mm
4	Duct aspect ratio (W/H)	10
5	Reynolds number (Re)	35,700 to 72,800
6	Angle of attack (α)	75°
7	Heat flux	1000 W/m ²

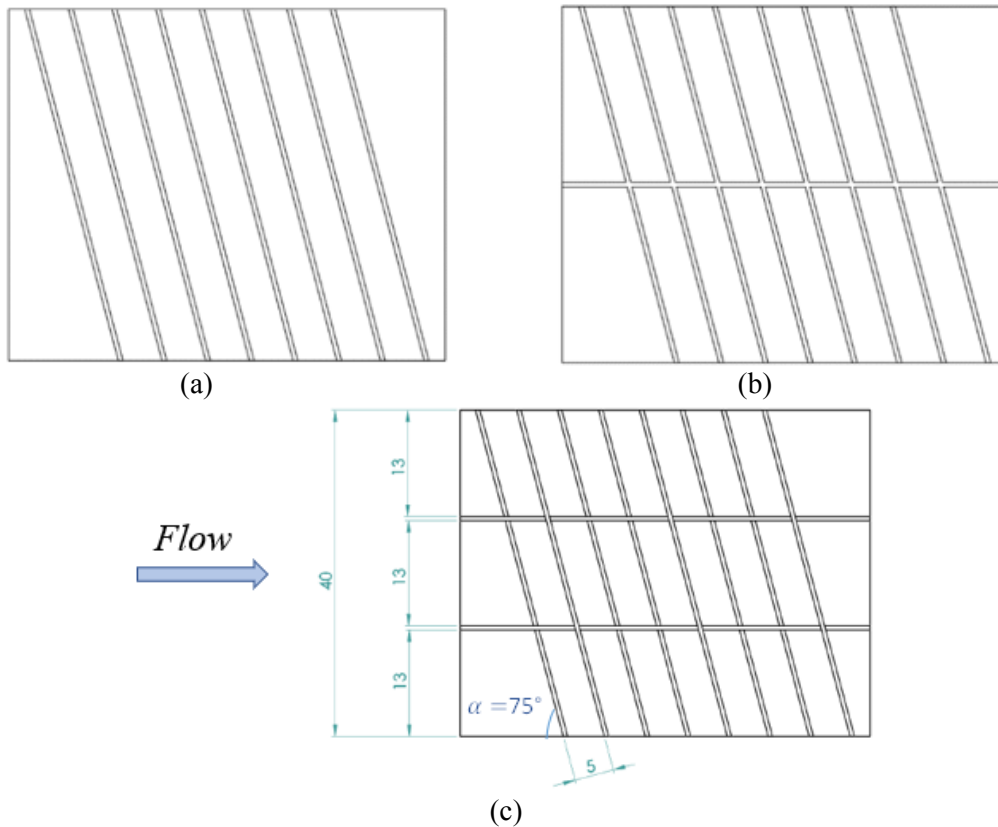


Figure 5. Roughened models; (a) Model 1, (b) Model 2 and (c) Model 3.

4. Data reduction

The logical calculation procedure of Nusselt number and friction factor had been carried out. Firstly, the heat flux was calculated from the power input to the heater. A part from the heater power was dissipated into conduction through the insulation of the bottom surface and radiation from the heating surface to the duct walls. These losses were estimated around 9 % of the total heater power input. While the biggest part of heat was transferred to the air flow by forced convection, and calculated as:

$$q_{conv.} = \frac{Q_{el} - Q_{loss}}{A_s} \quad (1)$$

where A_s is the top surface area of the test plate, and (Q_{el}) is the measured input power to the heater was estimated simply as:

$$Q_{el} = V \times I \quad (2)$$

The total heat loss (Q_{loss}):

$$Q_{loss} = Q_{cond.} + Q_{rad.} \quad (3)$$

where $Q_{cond.}$ is the heat loss by conduction, For $Q_{rad.}$ is the radiation heat transfer from the heating surface, estimated as:

$$q_{rad.} = F_b F_g \sigma A_s (T_s^4 - T_d^4) \quad (4)$$

where (σ) is the Stefan-Boltzmann constant and equal to $\sigma = 5.67 \times 10^{-8} \text{ W/m}^2 \text{ K}^4$, (F_g) is the geometry factor, and taken as one unity [7], while (F_b) is the emissivity factor and equal to $F_b = 0.3$ for aluminum. T_d is the duct surface temperature.

The local surface temperature of the test plate ($T_{s,x}$) and the local air bulk temperature ($T_{b,x}$), used to estimate the local heat transfer coefficient (h_x) as:

$$h_x = \frac{q_{conv.}}{(T_{s,x} - T_{b,x})} \quad (5)$$

The local flow bulk temperature ($T_{b,x}$) can be estimated by used the heat balance equation, by sequence as:

$$T_{b,x} = T_{b,x-\Delta x} + \frac{q_{conv.}(W.\Delta x)}{\dot{m}C_p} \quad (6)$$

Firstly, $T_{b,x-\Delta x}$ is the value of the measured inlet flow temperature of the test section, and the mass flow rate (\dot{m}) is obtained as ($\dot{m} = \rho u_m A_c$), where (u_m) is the mean velocity, and (A_c) is the cross-sectional area of the duct.

The local Nusselt number and Reynolds number based on the hydraulic diameter (D_h) were calculated by:

$$Nu_x = \frac{h_x D_h}{K_{air}} \quad (7)$$

$$Re = \frac{u_m D_h}{\nu} \quad (8)$$

The average Nusselt number (Nu) was calculated by averaging the local values of the Nusselt number along the whole plate length as:

$$Nu \approx \frac{\sum_{x=0}^x=L Nu_x}{L} \quad (9)$$

The friction factor (f) was evaluated as:

$$f = \left(\frac{\Delta P}{2 \rho u_m^2} \right) \left(\frac{D_h}{L} \right) \quad (10)$$

where ΔP is the pressure drop along the test section, and it was calculated by Digital Manometer, L is the distance between the two pressure taps, and ρ is the air density. The air properties were estimated at the mean temperature of flow (T_f):

$$T_f = \frac{(T_{in} + T_{out})}{2} \quad (11)$$

5. Uncertainty analysis

The accuracy of the experimental result depends on the precision of instruments and manufacturing accuracy of the instrument. Coleman and Steele [16], described the approximation methods that used to calculate the uncertainty, based on the ANSI/ASME standard. For an estimated parameter 'f' which is dependent on 'n'. The total uncertainty in 'f' is evaluated as summation of the participation of the measured parameter and evaluated as:

$$\delta f = \pm \sqrt{\sum_{j=1}^n \left(\frac{\partial f}{\partial x_j} \delta x_j \right)^2} \quad (12)$$

Where $\frac{\partial f}{\partial x_j}$ the sensitivity coefficient from each parameter is, δx_j is error contribution and δf is a total error. Percentages of uncertainties in the measurements of hydraulic diameter D_h , duct area, air velocity, flow mean temperature and electric power input were $\pm 0.02\%$, $\pm 0.125\%$, $\pm 0.967\%$, $\pm 2.2\%$, and $\pm 1.73\%$ respectively. Therefore, a total uncertainty was found for Reynolds number, heat transfer coefficient, Nusselt number and friction factor of $\pm 1.12\%$, $\pm 6.73\%$, $\pm 6.72\%$ and $\pm 2.14\%$, respectively.

6. Validation of experimental data

To validate experimental results, friction factor and average Nusselt number had been evaluated for smooth surface and compared with the values obtained by empirical equations. Equation 5-2 and 5-3 are used to calculate Nusselt number and friction factor, respectively. These equations utilized for turbulent flow and used by many researchers [14, 17, 18], for validation of the results;

Dittus-Boelter equation

$$Nu_s = 0.023 Re^{0.8} P^{0.4} \quad (13)$$

Modified Blasius equation

$$f_s = 0.085 Re^{-0.25} \quad (14)$$

The outcomes of the validation test for the comparison of the experimental and the theoretical values of the Nusselt number and friction factor as a function of the Reynolds number within a range from 35,700 to 72,800, is shown in Figure 6 (a) and (b), respectively. The average deviation estimated for investigated results for the Nusselt number and friction factor from those predicted values are 3.26% and 4.55%, respectively. These show a rationally good agreement for the experimental values of the Nusselt number and friction factor.

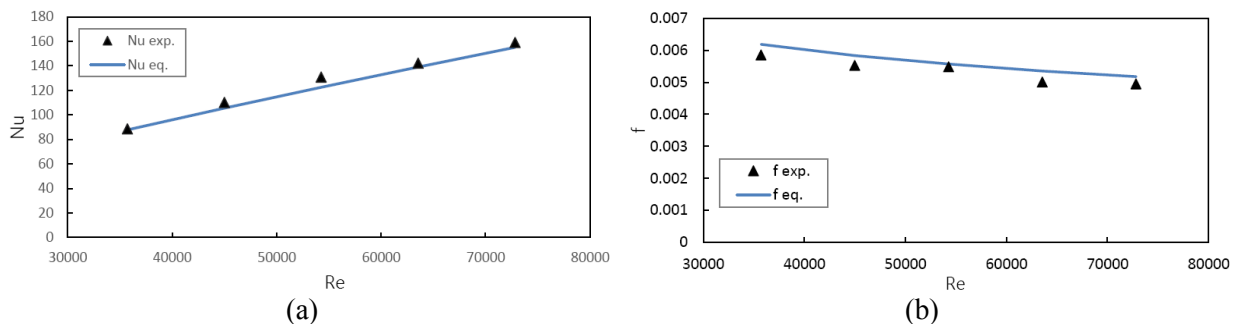


Figure 6. (a) Comparison of experimental and estimated values of Nusselt number of smooth ducts, (b) Comparison of experimental and estimated values of friction factor of smooth duct.

7. Results and discussion

7.1 Heat transfer

Figure 7 shows the values of the average Nusselt number for the different models as a function of Reynolds number. The results show that the Nusselt number for the Model 3 is the largest, thereafter that for the Model 2, and Model 1. Generally, it observed that, as the Reynolds number increases, the average Nusselt number also increases. This result is reasonable and it corresponds with the basics of forced convection heat transfer. This is because of the increasing of the heat transfer from the surface to the cooler fluid. Therefore, the local Nusselt number enhances with the increasing of Reynolds number directly. In case of, ribbed models, the Nusselt numbers is higher than that from smooth surface. This is due to disturbance occurs at the boundary layer due to the flow separation and reattachment, but with excessive pressure drops penalty.

To bring out the effect of the intersecting ribs clearly, the span-variation of the temperature along the test plate is presented in Figure 8, that clarify temperature distribution according to thermocouples' positions on heating surface (attached in Figure 8). It can observe clearly the decreasing of the surface temperature when added ribs to the smooth surface, which caused enhancement in heat transfer. Approximately, the surface temperature in the leading region of the inclined ribs is similar for both model 1 and 2, but reduced in model 3 due to the intersecting rib in the leading side, as shown in Figure 8 (Line 1). Then, the variation

of surface temperature for model 1, 2 and 3, began to appear clearly down to the trailing region, as shown in Figure 8 (Line 2, 3 and 4). However, at the trailing region of the inclined ribs, the heat transfer was locally augmented when added the intersecting ribs.

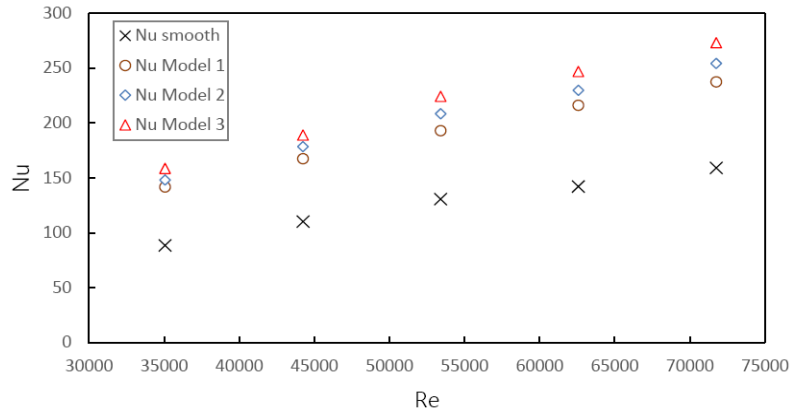


Figure 7. Average Nusselt number vs. Reynolds number for ribbed models.

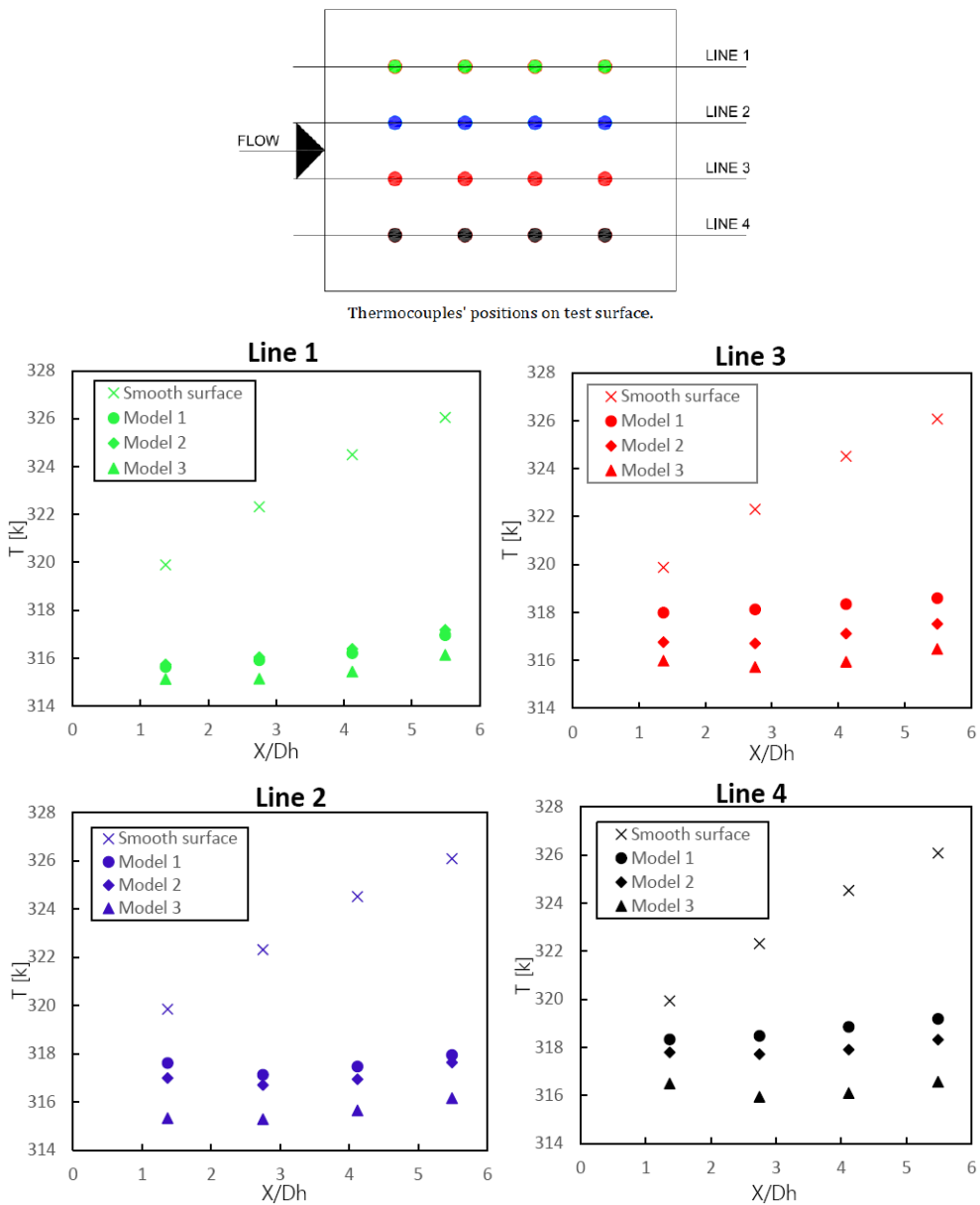


Figure 8. Local temperature distribution on test plate surface for different lines of ribbed models.

In the absence of an intersecting rib, the inclination angle of the rib with respect to flow generates counter-rotating secondary flow at the leading side corner of every rib. These vortices move immediately along the rib to the trailing side corner and, that causes span wise variation of heat transfer coefficient [5]. The strength of these vortices gradually diminished and their shape changed, during this moving from the leading side to the trailing side (see Figure 1). The moving vortices bring the working fluid in contact with leading edge, so increasing heat transfer rate while the trailing edge heat transfer is relatively low, as the vortices dissipated. This leads to an observed span-wise variation of heat transfer rate. For this reason, observed that the surface temperature for model 1 increased as approached to the trailing region.

Therefore, to overcome this disadvantage, longitudinal ribs were used with the inclined ribs in the intersection form. A single longitudinal rib was installed at the center of the plate with parallel to flow, this for Model 2, and two longitudinal ribs were used for Model 3. These cross ribs created additional vortices at the intersection points in addition to the primary vorticities which generated at the leading corner of the inclined rib, as shown in Figure 9. Therefore, the number of locations with enhanced heat transfer was doubled. Consequently, a locally enhanced heat transfer was observed in the trailing region of the inclined rib (see Figure 8), that showed the decreasing of surface temperature for different models in the line 4, also line 3 and 2 but with lower ratio relatively. Therefore, the Model 3 showed a highest heat transfer enhancement rather than Model 2, due to have more intersection points for two longitudinal ribs, which creates more vortices.

To compare the enhancement of the Nusselt number of the ribbed models with and without intersecting ribs relative to smooth surface. Figure 10 shows the average Nusselt number ratio (Nu / Nu_s) for the ribbed models as a function of the Reynolds number. It is found that the enhancement in the average Nusselt number is significantly affected by the intersecting ribs, due to the flow phenomenon as discussed previously. It can see that for any Reynolds number. The Nusselt number ratio is higher for models with intersecting ribs as compared to that of Model 1 (without intersecting ribs). Also, the Nusselt number ratio increases when added two intersecting ribs in the sides (Model 3) instead of one intersecting rib at the center (Model 1).

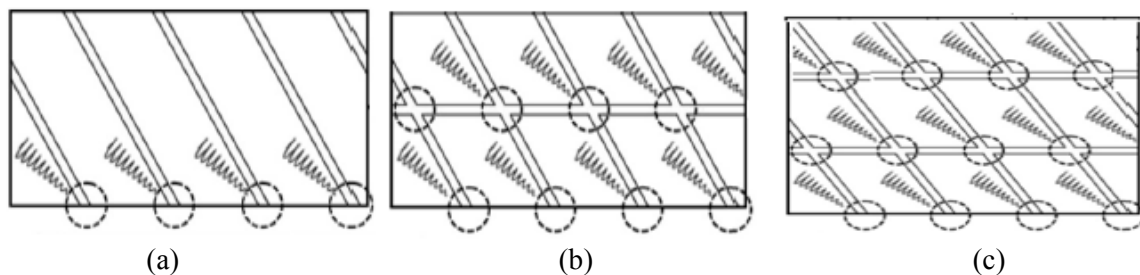


Figure 9. Vortex generations in case of (a) Model 1, (b) Model 2 and (c) Model 3.

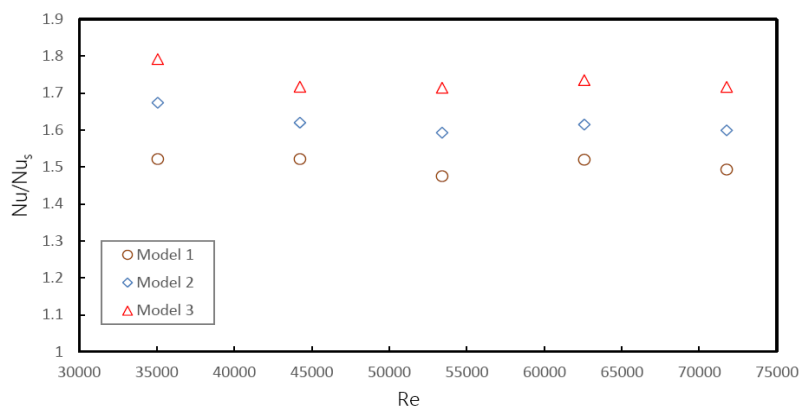


Figure 10. Nusselt number enhancement ratios (Nu/Nu_s) vs. Reynolds number for ribbed models.

7.2 Pressure drop results

The measured pressure drop along the length of the test section for the ribbed surface compared with the smooth surface, described as a function of Reynolds number, as shown in Figure 11. The pressure drop is increasing with increasing the Reynolds number due to the increasing of the flow turbulence.

In General, it can be observed that the adding of ribs increased the pressure drop for all three models, this is because of flow will stop entirely in front of the rib and causes extra pressure drops. For ribbed models, there is not large difference between them, especially at the low Reynolds number. It was found that that the maximum value of pressure drop is found at model 3 which also have the maximum value of Nusselt number, and then model 2 higher than model 1. This is a reasonable result due to the Intersecting ribs that cause more obstruction as shown in in Figure 12, that clarify the friction factor ratio (f/f_s) for the three models relative to the smooth surface, Where, f_s is average friction factor for the smooth channel. Hence, the Intersecting rib improve the heat transfer enhancement but with increasing in pressure drop penalty. It is therefore necessary to consider the Overall enhancement ratio to evaluate the optimum model.

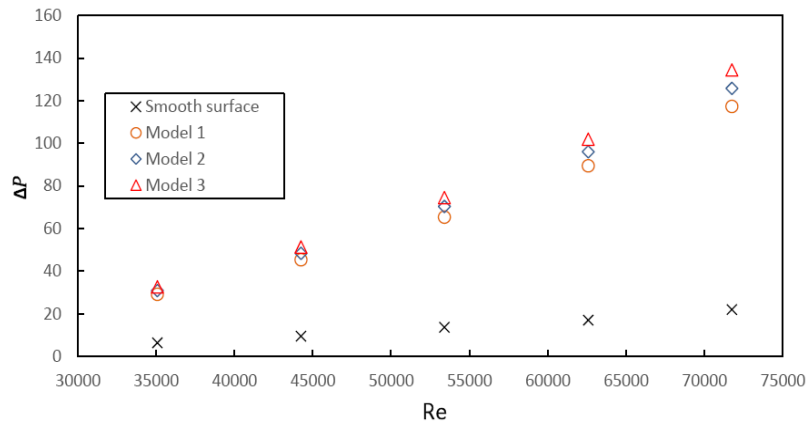


Figure 11. Pressure drop vs. Reynolds number for ribbed models.

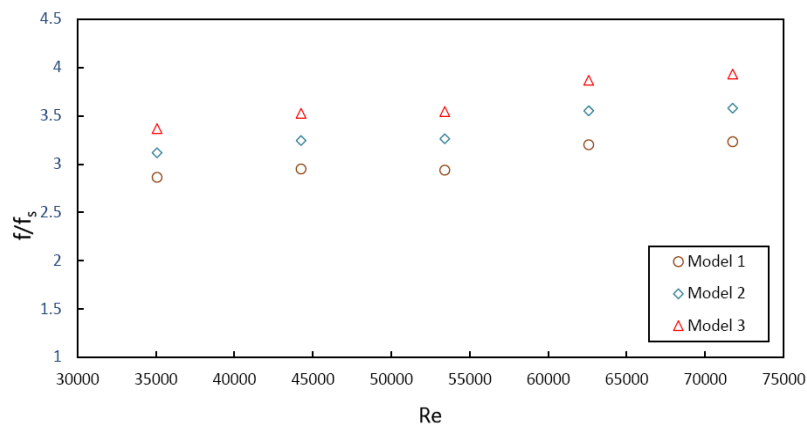


Figure 12. Friction factor ratio (f/f_s) vs. Reynolds number for ribbed models.

7.3 Overall thermal performance

It had been explained above that the Intersecting rib improve the heat transfer but accompanied with higher pressure drop penalty. Therefore, it is essential to estimate the overall thermal performance to determine the optimal model that achieve an enhancement in heat transfer with minimum pressure drop penalty. Lewis [19] presented an efficiency parameter ' η ' that represents the overall thermal performance, it defined as:

$$\eta = (Nu / Nu_s) / (f / f_s)^{1/3} \quad (15)$$

Figure 13 shows the variation of the overall thermal performance against Reynolds Number. It can be observed that the efficiency (η) for Model 3 is higher than those of the model 2 and 1. This clarify that the intersecting ribs showed excellent performance with inclined ribs. Thus, the hybridizing by intersection ribs with inclined ribs is considered useful technique to enhance the heat transfer, rather than using inclined ribs alone.

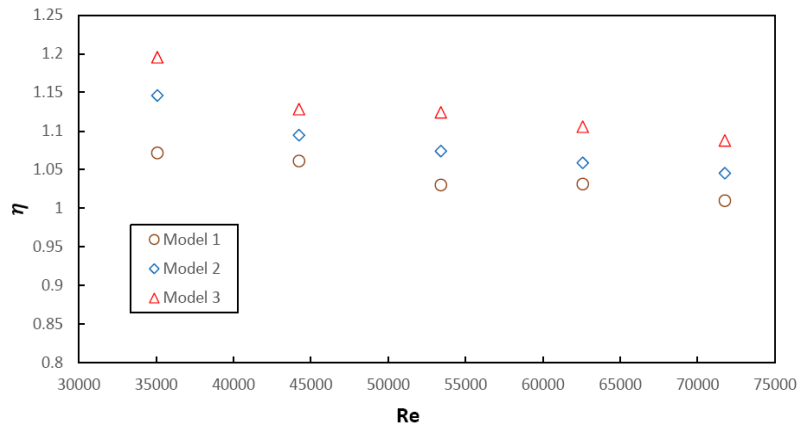


Figure 13. Overall Thermal Performance (η) vs. Reynolds Number for ribbed models.

8. Conclusion

Based on this experimental investigation for heat transfer and flow friction characteristics for turbulent flow in a rectangular duct roughened by longitudinal ribs with inclined ribs, the following conclusions have been recorded:

- 1) Intersecting ribs with the inclined ribs can be used for the heat transfer enhancement. The increasing in Nusselt number ratios (Nu / Nu_s) for a model with two intersected ribs (Model 3) and a model with one intersected rib (Model 2), compared to a model without intersecting ribs (Model 1), are 13.19% and 7.03%, respectively.
- 2) The penalty of added the intersecting ribs is increasing in pressure drop. The increase in friction factor ratios (f/f_s) for Model 3 and 2 compare to Model 1 are 16.76% and 9.36%, respectively.
- 3) The Model 3 with two Intersecting ribs mostly gives highest overall thermal performance rather than those of the Model 2 and 1.

Nomenclature

Latin Symbols

A_c	Cross-section area (W*H)
A_s	Top surface area of test plate
C_p	Specific heat at constant pressure
D_h	Hydraulic diameter of the duct
e	Rib height
H	Duct height
I	Current
L	Length of heated surface
\dot{m}	Mass flow rate
P	Pressure
p	Rib pitch
Q	Heat, Power
q	Heat flux
V	Voltage
W	Duct width

Greek Symbols

Δ	Difference in quantity
δ	Thickness
η	Overall thermal performance
ν	Kinematic viscosity
ρ	Density of air
α	Rib inclination angle

Dimensionless Numbers

Nu	Average Nusselt Number = $\frac{h D_h}{K_{air}}$
Re	Reynolds number = $\frac{u_m D_h}{\nu}$
e/D_h	Relative roughness height
p/e	Rib pitch to height ratio
f	Friction factor
Nu/Nu_s	Nusselt number enhancement ratio
f/f_s	Friction factor ratio

Subscripts

air	Air
b	Bulk Value
c	Cross-Section
cond	Heat transferred by conduction
conv	Heat transferred by forced convection
el	Electric power
in	Inlet
loss	Loss
m	Mean
out	Outlet
rad	Radiation
s	Test surface
x	Cartesian Coordinate

References

- [1] Ravi, B.V., Singh, P., and Ekkad, S.V. (2017). Numerical investigation of turbulent flow and heat transfer in two-pass ribbed channels. *International Journal of Thermal Sciences* 112, 31-43.
- [2] Aharwal, K., Gandhi, B., and Saini, J. (2008). Experimental investigation on heat-transfer enhancement due to a gap in an inclined continuous rib arrangement in a rectangular duct of solar air heater. *Renewable energy* 33, 585-596.
- [3] Taslim, M., and Liu, H. (2005). A Combined Numerical and Experimental Study of Heat Transfer in a Roughened Square Channel with 45° Ribs. *International Journal of Rotating Machinery* 2005, 60-66.
- [4] Satta, F., Simoni, D., and Tanda, G. (2012). Experimental investigation of flow and heat transfer in a rectangular channel with 45 angled ribs on one/two walls. *Experimental Thermal and Fluid Science* 37, 46-56.
- [5] Nagpure, S., Aharwal, K., and Bhagoria, J. 2015. "Effect of Artificial Roughness in Solar Air Heater-a Review,"..
- [6] Chung, H., Park, J.S., Park, S., Choi, S.M., Rhee, D.-H., and Cho, H.H. (2015). Augmented heat transfer with intersecting rib in rectangular channels having different aspect ratios. *International Journal of Heat and Mass Transfer* 88, 357-367.
- [7] Alfarawi, S., Abdel-Moneim, S., and Bodalal, A. (2017). Experimental investigations of heat transfer enhancement from rectangular duct roughened by hybrid ribs. *International Journal of Thermal Sciences* 118, 123-138.
- [8] Lei, J., Han, J.-C., and Huh, M. (2011). Effect of rib spacing on heat transfer in a two pass rectangular channel (AR= 2: 1) at high rotation numbers. In *ASME 2011 Turbo Expo: Turbine Technical Conference and Exposition (American Society of Mechanical Engineers)*, pp. 1329-1339.
- [9] Yang, W., Xue, S., He, Y., and Li, W. (2017). Experimental study on the heat transfer characteristics of high blockage ribs channel. *Experimental Thermal and Fluid Science* 83, 248-259.
- [10] Ghorbani-Tari, Z., Wang, L., and Sunden, B. (2013). 'Endwall Convective Heat Transfer around a Single Bluff Body in a Rectangular Channel. In *8th World Conference on Experimental Heat Transfer, Fluid Mechanics, and Thermodynamics 2013*.
- [11] Kim, D.H., Lee, B.J., Park, J.S., Kwak, J.S., and Chung, J.T. (2016). Effects of inlet velocity profile on flow and heat transfer in the entrance region of a ribbed channel. *International Journal of Heat and Mass Transfer* 92, 838-849.
- [12] Gao, T., Zhu, J., Liu, C., and Xu, J. (2016). Numerical study of conjugate heat transfer of steam and air in high aspect ratio rectangular ribbed cooling channel. *Journal of Mechanical Science and Technology* 30, 1431-1442.
- [13] Lu, B., and Jiang, P.-X. (2006). Experimental and numerical investigation of convection heat transfer in a rectangular channel with angled ribs. *Experimental Thermal and Fluid Science* 30, 513-521.
- [14] Ravi, R.K., and Saini, R.P. (2018). Nusselt number and friction factor correlations for forced convective type counter flow solar air heater having discrete multi V shaped and staggered rib roughness on both sides of the absorber plate. *Applied Thermal Engineering* 129, 735-746.
- [15] Aliaga, D., Lamb, J., and Klein, D. (1994). Convection heat transfer distributions over plates with square ribs from infrared thermography measurements. *International journal of heat and mass transfer* 37, 363-374.
- [16] Coleman, H.W., and Steele, W.G. (2018). *Experimentation, validation, and uncertainty analysis for engineers* (John Wiley & Sons).
- [17] Fayyedh, E.M., Hasan, M.R., and Mohammed, A.F. (2017). The Combined Effect of Rib with Single Large Eddy Break Up Devices on Flow and Heat Transfer Characteristic of Turbulent Flow in Rectangular Duct. *Al-Nahrain Journal for Engineering Sciences* 20, 281-291.
- [18] Kumar, A., and Layek, A. (2018). Nusselt number-friction characteristic for a twisted rib roughened rectangular duct using liquid crystal thermography. *Experimental Thermal and Fluid Science* 97, 205-217.
- [19] Lewis, M. (1975). Optimising the thermohydraulic performance of rough surfaces. *international Journal of Heat and Mass transfer* 18, 1243-1248.
- [20] Vishwakarma, V., Waghela, C., Wei, Z., Prasher, R., Nagpure, S.C., Li, J., Liu, F., Daniel, C., and Jain, A. (2015). Heat transfer enhancement in a lithium-ion cell through improved material-level thermal transport. *Journal of Power Sources* 300, 123-131.